Nickel Oxide growth on Si (111), c-Al_2O_3 & FTO/Glass by Pulsed Laser Deposition

V. E. Sandana[(a)], D. J. Rogers[(a)], F. Hosseini Teherani[(a)], P. Bove[(a)], R. McClintock[(b)] and M. Razeghi[(b)]

[(a)]Nanovation, 8 route de Chevreuse, Châteaufort, 78117, France.
[(b)]Center for Quantum Devices, ECE Department, Northwestern University, Evanston, Illinois 60208, USA

ABSTRACT

NiO was grown on Si (111), c-Al_2O_3 and FTO/glass substrates by pulsed laser deposition (PLD). X-Ray Diffraction (XRD) and scanning electron microscope (SEM) studies revealed that layers grown on c-Al_2O_3 were fcc NiO with a dense morphology of cubic grains that were strongly (111) oriented along the growth direction. The relatively low ω rocking curve linewidth, of 0.12°, suggests that there may have been epitaxial growth on the c-Al_2O_3 substrate. XRD and SEM indicated that films grown on Si (111) were also fcc NiO, with cubic grains, but that the grain orientation was random. This is consistent with the presence of an amorphous SiO_2 layer at the surface of the Si substrate, which precluded epitaxial growth. NiO grown at lower temperature (200°C) on temperature-sensitive FTO/glass substrates showed no evidence of crystallinity in XRD and SEM studies. After flash annealing in air, however, peaks characteristic of randomly oriented fcc NiO appeared in the XRD scans and the surface morphology became more granular in appearance. Such layers appear promising for the development of future dye-sensitised solar cell devices based on NiO grown by PLD.

Keywords: DSSC, NiO, FTO/Glass, Pulsed Laser Deposition, p-type semiconductor

INTRODUCTION

Face centred cubic (fcc) nickel oxide (NiO) is a direct [1] wide bandgap semiconductor material (reported Eg between 3.4 & 4.3eV, depending on measurement approach) [2-4] with excellent electrochemical stability. It also has a relatively high ionization potential and an elevated conduction band energy level. While stoichiometric NiO is electrically insulating, oxygen-poor NiO shows p-type conduction with a hole concentration that increases with oxygen content. This is generally attributed to positive charge compensation at Ni^{2+} vacancies. As a result of these properties, and their tunability, NiO has been investigated for a number of emerging uses including photocatalysis [5, 6], water treatment [7], electrochromics [8], UV photodetectors [9], thermoelectrics [10], chemical/gas sensing, [11], hole-transport/electron-blocking in organic electronic devices [12], supercapacitor electrodes, lithium ion battery anodes [13], fuel cells [14], hybrid LEDs [15] and p-type field effect transistors [16]. Of particular interest of late is the adoption of NiO as p-type semiconductor electrodes for novel tandem dye sensitized solar cells (DSSCs) in which the anode is a photoelectrode based on an n-type semiconductor (usually TiO_2 [17]) and the photocathode is a sensitized p-type SC. Indeed NiO is the only such p-type semiconductor found to give devices with significant photocurrent and photovoltage [18, 19]. Engineering of the stoichiometry, and the materials properties, are critical in determining the electrical and optical properties of NiO. Up till now, NiO photocathodes for DSSC applications have usually been synthesized by either solvothermal growth or electrodeposition [12, 20]. In this work, the potential of pulsed-laser deposition (PLD) [21-29] for the growth of NiO, which is better adapted for DSSC applications, is examined. In particular, good crystallinity, conductivity, a large surface-to-volume ratio and the possibility to function on an inexpensive and transparent glass superstrate are required. Indeed, the relatively high processing temperature necessary for high quality NiO synthesis by techniques other than PLD poses problems of compatibility with such temperature sensitive supports.

Oxide-based Materials and Devices V, edited by Ferechteh H. Teherani, David C. Look, David J. Rogers, Proc. of SPIE Vol. 8987, 89872P · © 2014 SPIE
CCC code: 0277-786X/14/$18 · doi: 10.1117/12.2057620

EXPERIMENT

NiO was deposited using PLD on Si (111), c sapphire (c-Al_2O_3) and Fluorine Tin Oxide (FTO) / glass by ablation of a sintered NiO target with a pulsed KrF excimer laser (248nm). Substrate temperature was 700°C for the Si (111) & c-Al_2O_3 growths and 200°C for the growth on (the more temperature-sensitive) FTO / glass. X-ray diffraction (XRD) studies were conducted with a Panalytical MRD high resolution diffractometer system. A Philips XL-30 Field Emission Gun-Scanning Electron Microscopy (FEG-SEM) was used to examine the surface morphology.

3. RESULTS & DISCUSSION

3.1 NiO Growth on Si (111)

Figure 1 shows typical SEM images for the growth on Si (111). A porous morphology with randomly oriented cubic crystal grains (slightly sub~100nm in scale) was observed. Cracks were also present, on the tens of microns scale, and there was a significant density (~ 5/100 μm^2) of polycrystalline particulates (ranging from ~500 nm to a few-microns in diameter) composed of similar cubic grains to those comprising the layer.

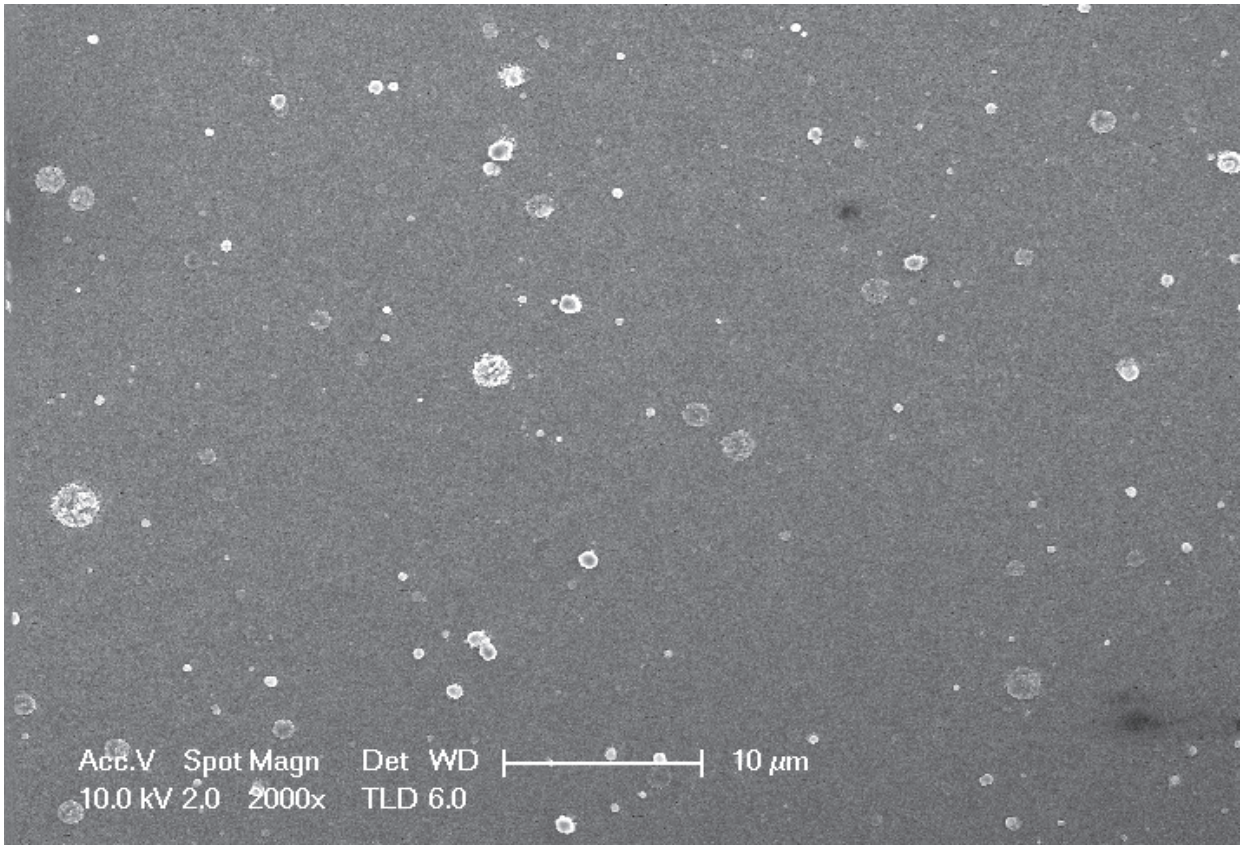

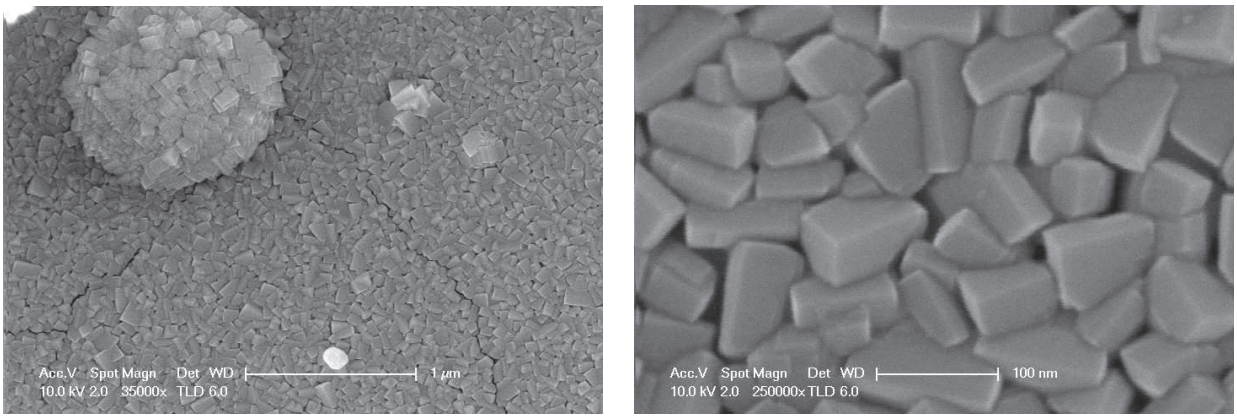

Figure 1. SEM images of NiO / Si (111).

XRD studies (Figure 2) showed relatively weak peaks indicative of the presence of randomly-oriented NiO [30].

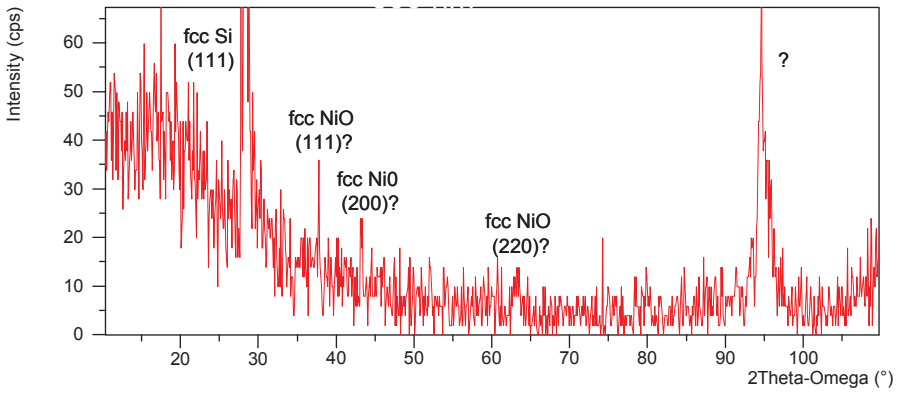

Figure 2. XRD 2θ–Ω scan of NiO / Si (111)

3.2 NiO Growth on c-Al_2O_3

Figure 3 shows typical SEM images for NiO grown on c-Al_2O_3.

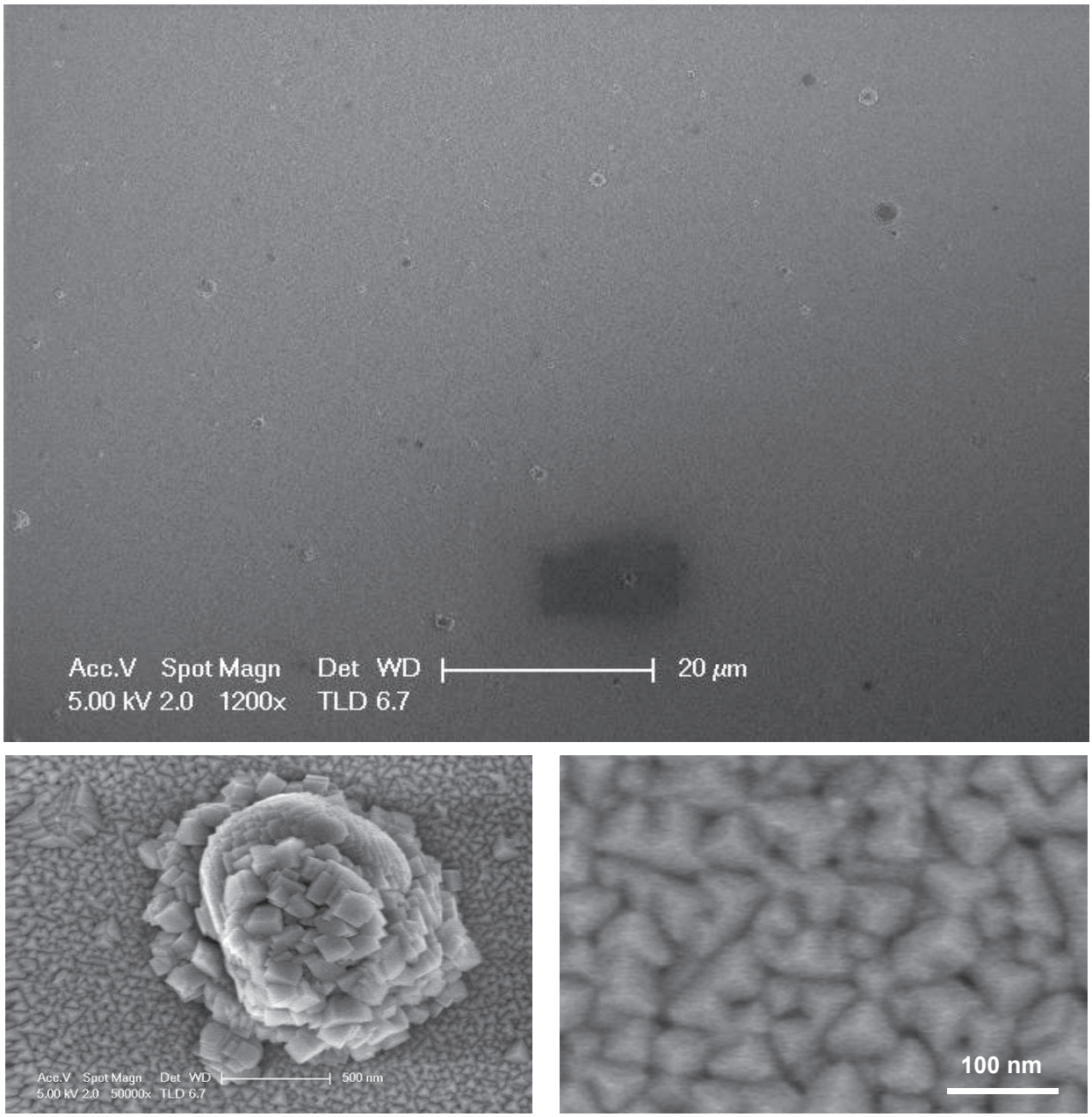

Figure 3. SEM images for NiO growth on c-Al_2O_3

As for the growth on Si (111), sub~100nm cubic crystal grains are observed and there is a density of ~ 1/100 μm^2 of polycrystalline particulates (ranging from ~500 nm to a few-microns in diameter) composed of cubic grains, which are similar to those in the layer. Unlike the growth on Si (111), however, the film morphology itself is dense (non-porous), no cracks are apparent and the grains exhibit a preferential (111) alignment along the film growth direction.

Figure 4 shows the corresponding XRD 2θ–Ω scan for the NiO growth on c-Al_2O_3.

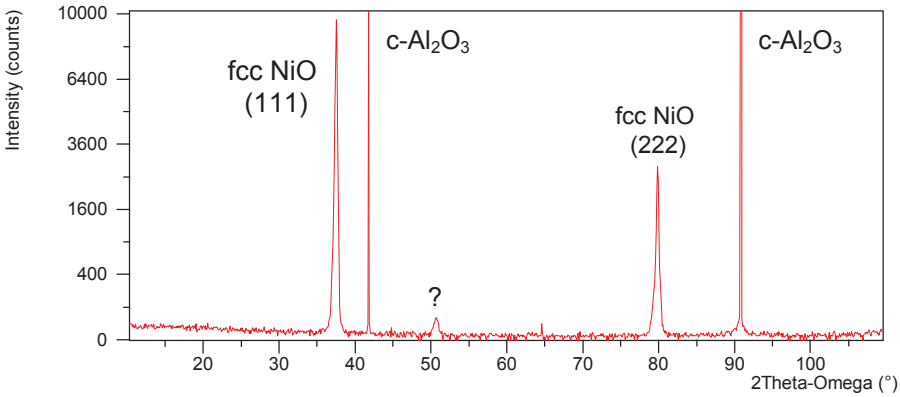

Figure 4. XRD 2θ–Ω scan for NiO growth on c-Al_2O_3

The presence of pronounced (111) and (222) peaks confirms the presence of fcc NiO with a strong preferential (111) orientation [30]. The XRD ω rocking curve for the (111) peak of the NiO / c-Al_2O_3 is shown in Figure 5.

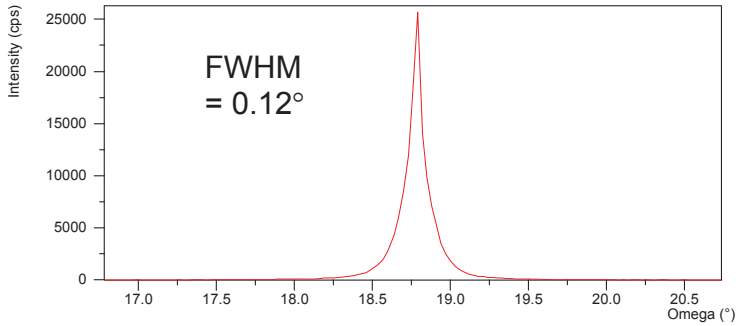

Figure 5. XRD Ω rocking curve for the (111) peak of NiO grown on c-Al_2O_3

The rocking curve has a FWHM of 0.12°, which is indicative of a relatively small dispersion in the crystallographic orientation about the (111) direction and is consistent with the preferential orientation of the grains in the SEM images. These findings suggest that there may have been epitaxial growth of fcc NiO on the c-Al_2O_3 substrate.

Electrical resistivity was measured for NiO/Al_2O_3 with the 4 co-linear probes method. The measured value of ~90 Ω.cm was relatively high. That could be related to low oxygen content and/or the porosity/cracks in the film [1].

3.3 NiO Growth on FTO / glass

Figure 6 shows the XRD 2θ–Ω scan for the NiO grown on FTO / glass.

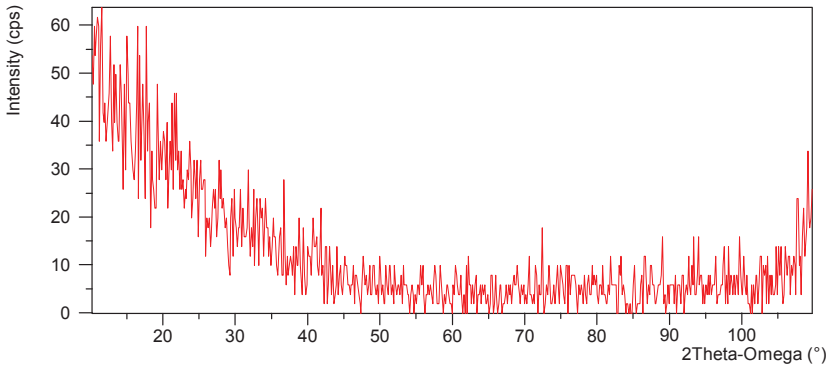

Figure 6. XRD 2θ–Ω scan for the NiO grown on FTO / glass.

No significant peaks are revealed by the scan.

Figure 7 shows SEM images of the NiO (as grown) on FTO/Glass.

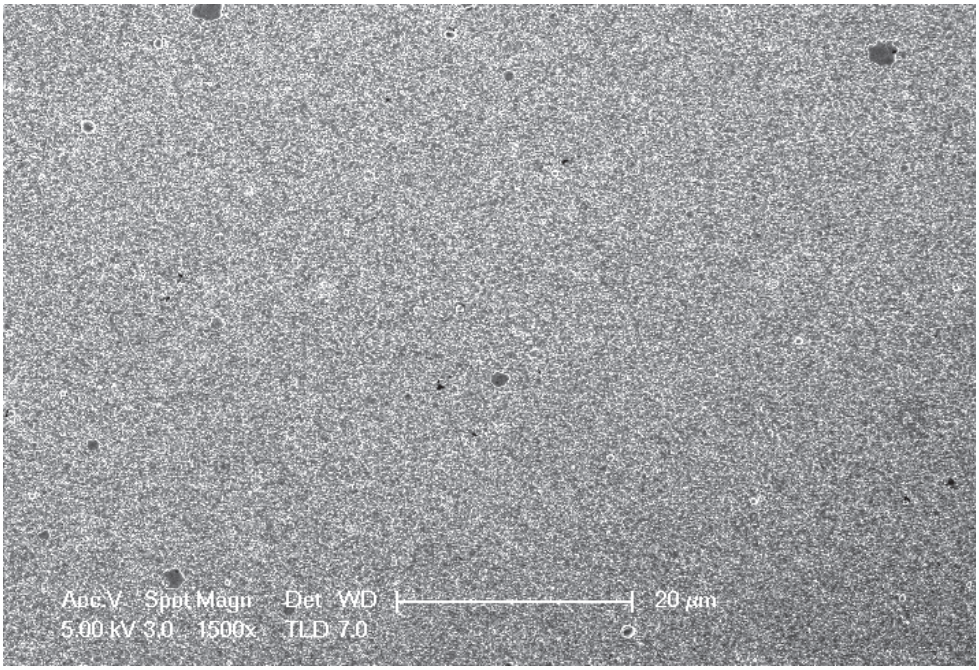

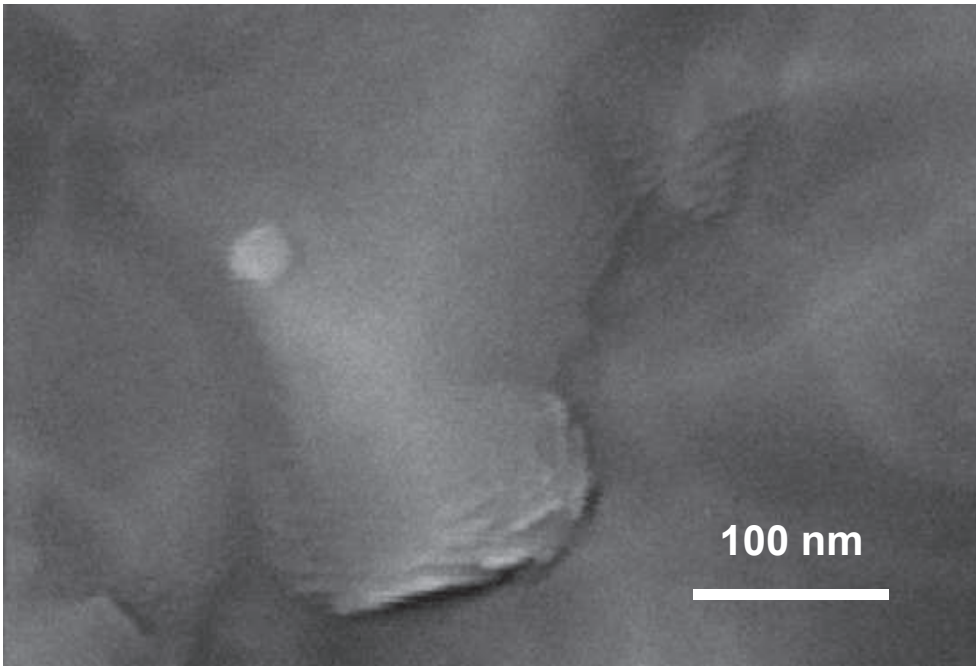

Figure 7. SEM images of the as-grown NiO on FTO / glass.

Although the lower magnification image suggests a certain granularity, higher magnification images do not reveal the distinct grain boundaries or faceting that would be expected for crystallographic grains. No cracks were apparent and there were relatively few particulate-like features. Based on these XRD and SEM results, it was inferred that the NiO layer on FTO / glass was either amorphous or very poorly crystallised.

Rapid thermal processing was employed, therefore, in order to try and (better) crystallise the layer. The NiO/FTO/glass was air annealed in a tubular furnace for 1 minute at 600°C.

Figure 8 shows SEM images of the NiO / FTO / glass after post-annealing.

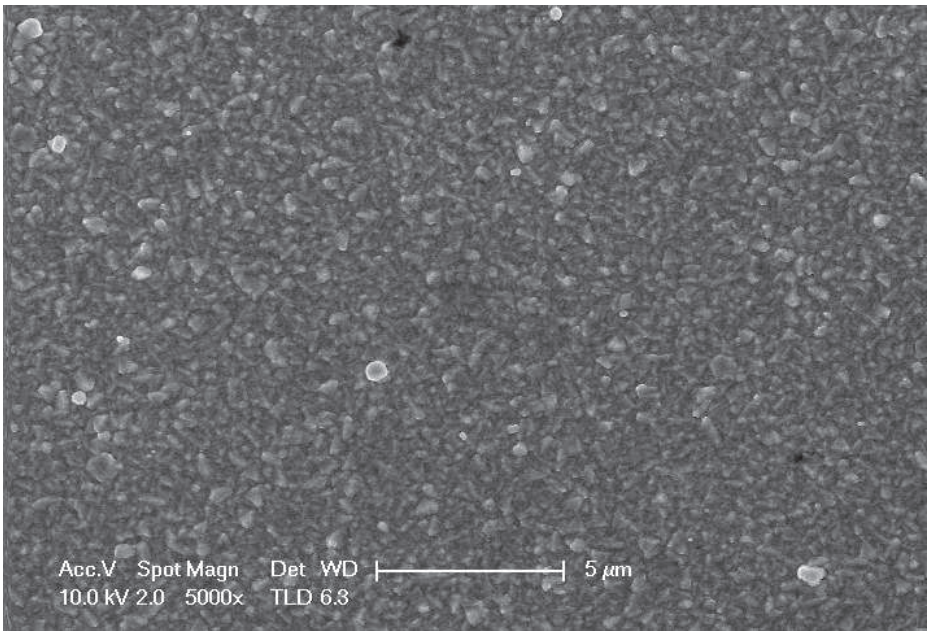

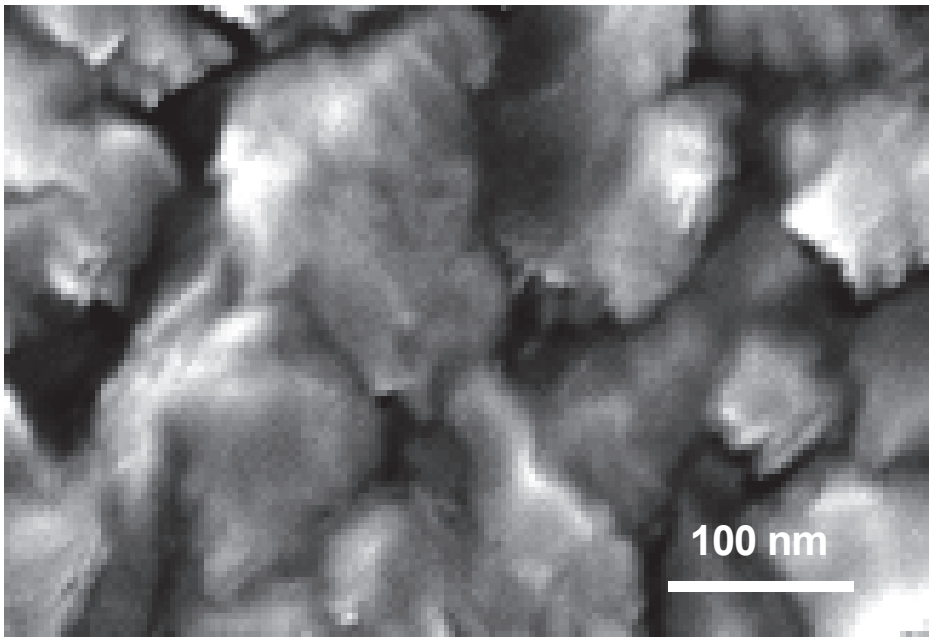

Figure 8. SEM images of NiO / FTO / glass after post-annealing in air

The images reveal a modified surface morphology after post-annealing with a more porous structure and small, grain-like features. Figure 9 shows the corresponding XRD 2θ–Ω scan for the NiO / FTO / glass after post-annealing in air.

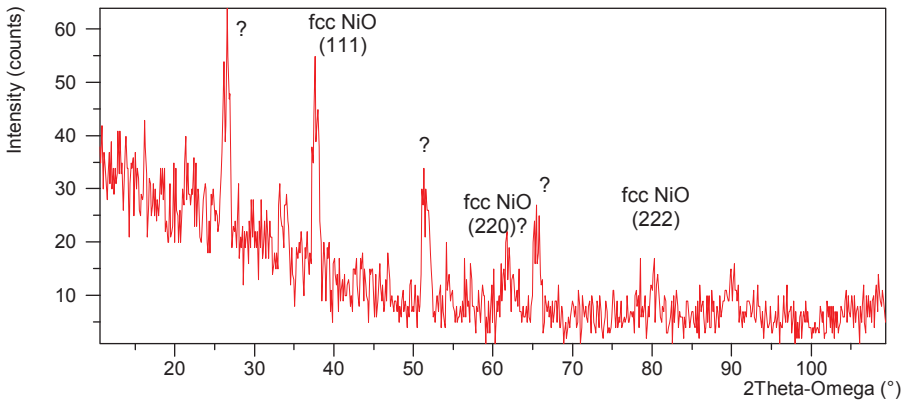

Figure 9. XRD 2θ–Ω Scan of NiO/FTO/glass post-annealing

Several peaks have appeared, which were not present in the scan prior to annealing, and which are indicative of randomly oriented fcc NiO on FTO [31].

CONCLUSIONS

NiO films were grown at 700°C on Si (111) and c-Al_2O_3. XRD and SEM studies revealed that layers grown on c-Al_2O_3 were fcc NiO with a dense morphology of cubic grains that were strongly (111) oriented along the growth direction. The relatively low ω rocking curve linewidth figure, of 0.12°, suggests that there may have been epitaxial growth on the c-Al_2O_3 substrate. XRD and SEM indicated that films grown on Si (111) were also fcc NiO, with cubic grains, but that the

grain orientation was random. This is consistent with the presence of an amorphous SiO_2 layer at the surface of the Si substrate, which precluded epitaxial growth.

NiO grown on temperature-sensitive FTO/glass substrates at 200°C showed no evidence of crystallinity in XRD and SEM studies. After annealing for 1 minute at 600°C, however, peaks characteristic of randomly oriented fcc NiO appeared in the XRD scans and the surface morphology became more granular in appearance. Such layers appear promising for the development of future DSSC devices based on NiO grown by PLD.

Acknowledgements

The authors wish to thank the CTU at IEF/UPSUD for access to the SEM / XRD facilities and to the ANR for the funding of the « POSITIF » research project.

REFERENCES

[1] S. Chakrabarty and K. Chatterjee Journal of Physical Sciences, 13 (2009) 245
[2] P. S. Patil & L. D. Kadam (2002) Appl Surf Sci 199:211–221
[3] S. Huffner S (1994) Adv Phys 43:183
[4] L. Ai et al. Applied Surface Science 254 (8), (2008) 2401
[5] C.G. Granqvist, Handbook of Inorganic Electrochimics Materials, Elsevier, Amsterdam, 1995.
[6] Z. Zhai et al. Nanoscale (2012) 4 , 547
[7] Xiaowei et al. J. Mater. Chem. (2012) 22 , 14276
[8] A. Azens et al. Solid State Ionics 113–115, (1998) 449
[9] H. Ohta et al. Thin Solid Films 445, 2, (2003), 317
[10] W. Shin & N. Murayama Materials Letters 45, 6, (2000) 302
[11] A. Dirksen, et al. Sensors and Actuators B: Chemical 80, 2, 20 (2001) 106
[12] S. Bai et al. Adv. Energy Mater. (2013) 1, online publication, DOI 10.1002aenm.201301460
[13] A. Vu et al. Adv. Energy Mater. (2012) 2, 1056
[14] P. I. Cowin, et al. Adv. Energy Mater. (2011) 1, 314
[15] Y. Y. Xi et al. Appl. Phys. Lett. 92 (2008) 113505- 1
[16] H. Shimotani et al. Appl. Phys. Lett. 92 24 (2008) 242107
[17] S. Zhang et al. Energy Environ. Sci. 6 (2013) 1443-1464.
[18] A. Nakasa et al. Chem.Lett. 34 (2005) 500.
[19] F. Odobel et al. Coord. Chemi. Rev. 256 (2012) 2414– 2423.
[20] M. Awais et al. Chem. Electro. Chem, 2, (2014) 384 – 391
[21] D. Rogers et al. Proc. of SPIE Vol. 7217 (2009) 72170F-1.
[22] V. E. Sandana et al. Phys. Status Solidi C 10 (2013) No. 10, 1317–1321.
[23] B Sasi et al. Nanotechnology 18 (2007) 115613 (9pp)
[24] S. Pilban Jahromi et al. Journal of Nanomaterials Volume 2012, Article ID 173825, 4 pages
[25] A. Largeneau et al. U.P.B. Sci. Bull., Series A, Vol. 73, Iss. 3, 2011
[26] I. Bouessay et al. Applied Surface Science 186 (2002) 490-495
[27] P. Bılkova et al. Appl. Phys. A 79, 1061–1065 (2004)
[28] M. Stamataki et al. Phys. Stat. Sol. (a) 205, No. 8, 2064–2068 (2008)
[29] H. Wang et al. Electrochemistry Communications 18 (2012) 92–95
[30] X. Sun et al. Adv. Energy Mater. (2013) online publication, DOI: 10.1002/aenm.201300912
[31] H. B. Yang et al. Adv. Mater. Interfaces (2014) online publication, DOI: 10.1002/admi.201300110